International Journal of Mass Spectrometry 309 (2012) 109–117

Contents lists available at SciVerse ScienceDirect

International Journal of Mass Spectrometry

journal homepage: www.elsevier.com/locate/ijms

High precision tungsten isotope measurement by thermal ionization mass spectrometry

Mathieu Touboul*, Richard J. Walker

Department of Geology, University of Maryland, College Park, MD 20742, USA

ARTICLE INFO

Article history:
Received 21 June 2011
Received in revised form 31 August 2011
Accepted 31 August 2011
Available online 10 September 2011

Keywords:
Tungsten isotope
Extinct nuclide
^{182}W
Thermal ionization
Triton
N-TIMS

ABSTRACT

We describe a new technique for measuring the isotopic abundance of ^{182}W with improved precision in natural silicate samples. After chemical purification of W through a four-step ion exchange chromatographic separation, the W isotopic composition is measured as WO_3^- by negative thermal ionization mass spectrometry using a *Thermo-Fisher Triton* instrument. Amplifier biases are cancelled by using amplifier rotation, and Faraday cup biases are monitored by using a cup configuration that allows two-line data acquisition. Data are initially corrected for oxide interferences, assuming a predefined O isotope composition, and for mass fractionation, by normalization to ^{186}W/^{184}W or ^{186}W/^{183}W, using an exponential law. Despite these corrections, isotopic ratios exhibit small but strongly correlated variations. This second-order effect may reflect a mass dependent change of O isotope composition in the measured W (and Re) oxides, and is corrected by normalization to ^{183}W/^{184}W using a linear law. Repeated analysis of an *Alfa Aesar* W standard (n = 39), and of three dissolutions of a La Palma (Canary Islands) basalt, applying the double normalization procedure, demonstrate external reproducibility of ^{182}W/^{184}W within ±4.5 ppm (2σ SD). Repeated measurement of a gravimetrically prepared mixture of a natural W standard and a ^{182}W enriched spike shows that differences in ^{182}W/^{184}W of ∼10 ppm can be well resolved using this method. The external reproducibility of ±4.5 ppm is ∼5 times more precise than conventional W isotope measurements by MC-ICP-MS. The new technique constitutes an ideal tool for investigating the W isotope composition of terrestrial rocks for potential contributions from the core, and late accreted extraterrestrial materials.

Published by Elsevier B.V.

1. Introduction

Over the past two decades, the short-lived ^{182}Hf–^{182}W chronometer ($T_{1/2}$ = 8.9 Myr; [1]) has been widely used for dating early Solar System processes, due to the unique geochemical properties of the system. Tungsten is a siderophile (iron-loving) element, and as such, it is largely (but not completely) extracted from the silicate mantles of planetary bodies during segregation of metallic cores [2–8]. Hafnium, in contrast, is lithophile (silicate-loving) and is wholly retained in the silicate portion of planetary bodies. Therefore, determination of the abundance of the daughter nuclide, ^{182}W, relative to other stable, non-radiogenic W isotopes (e.g., ^{184}W) is of special interest for constraining the timing of planetary core formation.

All terrestrial rocks investigated to date [9–13] have been characterized by ^{182}W/^{184}W ratios that are ∼200 ppm more radiogenic than primitive, undifferentiated meteorites, e.g., chondrites [14–17]. The difference between the terrestrial rocks and chondritic meteorite compositions has been interpreted as evidence of the early formation of the Earth's core, less than 30 Myr after the initial formation of the Solar System [14,16,18,19]. The difference also implies that the Earth's core is a W-rich reservoir with a ^{182}W/^{184}W that is likely ∼350 ppm lower than terrestrial silicates. Because Hf and W are also fractionated by magma ocean crystallization, partial melting of the silicate mantle, and subsequent crystal-liquid fractionation processes [20], the absence of significant W isotopic variations among terrestrial rocks suggests either that the differentiation of the Earth's mantle occurred more than 60 Myr after Solar System formation, after ^{182}Hf became extinct, or that traces of primitive crustal or mantle reservoirs that formed earlier have been erased by convective mixing. The late formation of the Moon (>50 Myr after Solar System formation), ostensibly by a giant impact [21–23] provides supporting evidence for late-stage homogenization of W isotopes in the Earth's mantle.

Despite the likely homogenization of W isotopes in the mantle following the putative giant impact that generated the Moon, small W isotope heterogeneities might have been generated after ^{182}Hf was no longer extant as a result of the late accretion of materials with either more ^{182}W-depleted or enriched isotopic compositions

* Corresponding author.
E-mail addresses: mtouboul@umd.edu (M. Touboul), rjwalker@umd.edu (R.J. Walker).

1387-3806/$ – see front matter Published by Elsevier B.V.
doi:10.1016/j.ijms.2011.08.033

[24], or as a result of core–mantle interactions [10]. The contributions of extraterrestrial or core-derived materials to portions of the mantle that may be sampled by volcanic systems would be small, but could potentially be resolved with sufficiently high precision measurements.

In the late 1990s, the first high-precision W isotopic compositions of geological materials were measured for iron meteorites [25,26] using negative thermal ionization mass spectrometry (N-TIMS), a technique developed earlier by Heumann et al. [27] and Völkening et al. [28]. Repeated measurements of W standards on first generation, multiple-collector TIMS instruments yielded external reproducibility on $^{182}W/^{184}W$ ratios of ~100 ppm (2σ SD). The N-TIMS technique was then quickly abandoned with the advent of multiple-collector inductively coupled plasma mass spectrometry (MC-ICP-MS) (e.g. [29]). The MC-ICP-MS technique proved to be more sensitive and more reproducible than N-TIMS, and currently remains the most common method employed for the measurement of W isotopes. Typical, single-analysis external precision for this technique is currently ~±25 ppm.

Here we present a refined N-TIMS technique for the measurement of W isotopes, using a *Thermo-Fisher Triton* to achieve external reproducibility of better than ±5 ppm on $^{182}W/^{184}W$ ratios measured for natural samples. An improved chemical procedure for W extraction and extensive purification of W from large quantities of silicate rock required for the N-TIMS measurement is provided, along with a detailed measurement protocol that includes oxide interference corrections and a double normalization procedure. Accuracy and external reproducibility of the method were defined via repeated measurement of our *Alfa Aesar* standard, a gravimetrically prepared W standard-^{182}W spike mixture, and multiple dissolutions of a La Palma (Canary Islands) basalt [30]. The improvement to precision will permit a more rigorous search for W isotope variations in terrestrial rocks than has been previously achieved.

2. Sample preparation

2.1. Sample dissolution

Three to ten grams of the La Palma basalt [30] were dissolved in a closed (250 ml) *Savillex* Teflon beaker using 100 ml of a 5:1 mixture of concentrated HF–HNO_3 (all acids used in this study were high purity, sub-boiling-distilled in Teflon), on a hot plate at 180 °C for a week. Samples were then gently dried down under UV lamps. The resulting fluorides were progressively broken down via subsequent, repeated additions of 30% H_2O_2 (1 ml) and concentrated HNO_3 (40 ml) on a hot plate at 120 °C. Samples were dried down between each treatment. The samples were then converted to chloride form by repeated dissolutions and dry downs in 6 M HCl. Although not critical here, dissolution was never completely achieved. After the addition of 40 ml of 1 M HCl–0.1 M HF to the final residues, the closed Teflon beakers were put on a hot plate at 120 °C for 24 h, allowing additional fluorides to precipitate. The samples were then allowed to cool and were then subjected to 30 min of ultrasonification. The samples were centrifuged and the supernatants were removed and saved for the ion exchange chromatography procedure. The remaining fluorides (~30 ml of precipitates) were rinsed with 20 ml of 1 M HCl–0.1 M HF. The closed Teflon beakers were put on a hot plate at 120 °C for 2 h, then in an ultrasonic bath for 30 min prior to a second centrifugation. The 20 ml supernatant resulting from this step was also saved for ion exchange chromatography, where it was subsequently used to rinse W from the resin remaining after of the first extraction. This step was repeated one more time.

Table 1
Four-step ion exchange chromatography procedure for W purification.

Acid	Volume (ml)	Step
1st step: 4 *Biorad* columns filled with 15 ml AG50-X8. 200–400 mesh		
6 M HCl	60	Resin cleaning
4 M HF	15	Resin cleaning
6 M HCl	15	Resin cleaning
4 M HF	15	Resin cleaning
6 M HCl	15	Resin cleaning
H_2O	15	Resin cleaning
1 M HCl–0.1 M HF	15 + 15	Equilibration
1 M HCl–0.1 M HF	10 + 5 + 5	Load
1 M HCl–0.1 M HF	5	Rinse W
2nd step: 4 *Biorad* columns filled with 2 ml AG1-X8. 100–200 mesh		
7 M HNO_3	10	Resin cleaning
6 M HNO_3–0.2 M HF	10	Resin cleaning
6 M HCl–1 M HF	10	Resin cleaning
0.5 M HCl–0.5 M HF	10	Resin cleaning
0.5 M HCl–0.5 M HF	10 + 10	Equilibration
0.5 M HCl–0.5 M HF	15	Load
0.5 M HCl–0.5 M HF	10	Rinse matrix
H_2O	2 + 2 + 2	Rinse HF
3.6 M HAc–8 mM HNO_3–1% H_2O_2	60	Ti elution
9 M HAc	2 + 2	Rinse Ti
6 M HCl–0.01 M HF	6	Hf elution
6 M HCl–1 M HF	12	W elution
3rd step: 1 *Biorad* columns filled with 2 ml AG1-X8. 100–200 mesh		
7 M HNO_3	10	Resin cleaning
6 M HNO_3–0.2 M HF	10	Resin cleaning
6 M HCl–1 M HF	10	Resin cleaning
0.5 M HCl–0.5 M HF	10	Resin cleaning
0.5 M HCl–0.5 M HF	10 + 10	Equilibration
0.5 M HCl–0.5 M HF	1	Load
0.5 M HCl–0.5 M HF	10	Rinse matrix
H_2O	2 + 2 + 2	Rinse HF
3.6 M HAc–8 mM HNO_3–1% H_2O_2	100	Ti elution
9 M HAc	2 + 2	Rinse Ti
6 M HCl–0.01 M HF	6	Hf elution
6 M HCl–1 M HF	12	W elution
4th step: 1 *Biorad* columns filled with 140 μl AG1-X8. 100–200 mesh		
7 M HNO_3	1	Resin cleaning
6 M HNO_3–0.2 M HF	1	Resin cleaning
6 M HCl–1 M HF	1	Resin cleaning
0.5 M HCl–0.5 M HF	1	Resin cleaning
0.5 M HCl–0.5 M HF	1 + 1	Equilibration
0.5 M HCl–0.5 M HF	0.1	Load
0.5 M HCl–0.5 M HF	0.2	Rinse matrix
1 M HF	0.5	Rinse matrix
H_2O	0.2 + 0.2	Rinse HF
6 M HCl–0.01 M HF	0.3	Hf elution
6 M HCl–1 M HF	1	W elution

2.2. Ion exchange chromatography

A four-step ion exchange chromatographic procedure was adapted from previous studies [23,31]. The complete procedure is designed to separate W from the large amount of silicate sample initially processed, then to highly purify the liberated W (Table 1). The first step uses AG50WX8 *Biorad* cation exchange resin (200–400 mesh). The sample is picked up in 40 ml of 1 M HCl–0.1 M HF, then split into four equal aliquants. Each aliquant is added to a separate column (*Biorad*, 1.5 cm × 12 cm) that is packed with 15 ml of resin. In the anionic form loaded onto the columns (WO_3^-), W is not retained on the resin, in contrast to major cations. Hence, the 40 ml loading volume, passed through each of the four columns, is directly collected together in one single 250 ml *Savillex* Teflon beaker. Any remaining W is then rinsed from the four columns by sequentially passing each of the 2 aliquants of 5 ml of 1 M HCl–0.1 M HF, derived from the two fluoride rinses (above), and collected in the same 250 ml beaker. This step separates the W from most of the sample matrix. The 80 ml sample solution obtained is then dried down under UV lamps.

In the second step, W is largely isolated from Ti, Hf, and other high field strength elements. The sample residues, dissolved in 4.5 ml of 0.5 M HCl–0.5 M HF, are loaded onto *Biorad* columns (0.8 cm × 12 cm) packed with 2 ml of AG1X8 *Biorad* anion resin (100–200 mesh). The resin bed is rinsed with 4 ml of 0.5 M HCl–0.5 M HF, then traces of HF are eliminated by rinsing the columns 3 times with 2 ml of high purity water. Titanium is eluted from the column by passing 60 ml of 3.6 M acetic acid (HAc)–8 mM HNO_3–1% H_2O_2 and rinsed with 9 M HAc. By passing 6 ml of 6 M HCl–0.01 M HF, Hf is removed from the column. Tungsten is then eluted using 12 ml of 6 M HCl–1 M HF. Solutions from the four columns are collected together in one single 250 ml beaker and dried down afterwards.

The third step provides further separation of W from Ti, Hf and other high field strength elements. This step is similar to the second step, but it involves only one column containing 2 ml anion resin, a smaller loading volume (1 ml) and a longer Ti elution (100 ml). Tungsten is eluted into a 15 ml *Savillex* Teflon beaker.

The fourth step, using a column filled with 140 μl of AG1X8 *Biorad* anion resin (100–200 mesh), is designed as a final purification. Samples, dissolved in 100 μl of 0.5 M HCl–0.5 M HF, are loaded onto a small column. The column is then rinsed with 200 μl of 0.5 M HCl–0.5 M HF, and 500 μl of HF 1 M. Any remaining Hf is eluted with 300 μl of 6 M HCl–0.01 M HF, and W is then collected via elution of 1 ml of 6 M HCl–1 M HF in a 15 ml *Savillex* Teflon beaker. After evaporation, W residues are repeatedly redissolved in 30 μl of a concentrated HNO_3–H_2O_2 mixture (2:1), then dried down, in order to remove organics.

The entire four-step ion exchange procedure efficiently separates W from major elements such as Si, Ca and Fe, as well as from elements that might inhibit W, thermal ionization, such as Ti. The separation also removes elements that might introduce isobaric interferences on W masses in the mass spectrometer, such as Os, Ta, Hf and the rare earth elements.

Upon completion of the chromatographic separation, a small aliquot (~0.5%) of the sample is separated for analysis using an ICP-MS to assess elemental purity and determining the chemical yield of each sample. The yield of this 4-step ion exchange procedure is typically ~80%. No significant impurity of potentially interfering elements, such as Hf, Ta, Re and Os, have been detected. The total procedural blank for W never exceeds 10 ng, and is inconsequential for the measurements reported here.

3. Mass spectrometry

3.1. Instrumentation and data acquisition protocol

Approximately 1.5 μg of W is loaded in 1 μL of 1 M HNO_3 onto an outgassed single Re filament that is heated with a current of 0.5 A. Tantalum and Pt filaments were also initially tried but they were not as efficient as Re filament for ionizing W, as previously noted [25,26,28]. A major disadvantage of using Re filaments is the generation of ^{185}Re trioxide that leads to isobaric interferences on ^{186}W trioxide. However, ReO_3^- ionizes most efficiently at much lower temperatures than W, and the Re signal typically drops from >1 V to about 80 mV by slowly (20 °C/min) warming up the filament to the run conditions for W (typically 1330–1350 °C). The ionization efficiency for WO_3^- is enhanced by covering the W deposit with 5 μg each of La and Gd oxide. These elements act as electron emitters. Oxide formation is also enhanced by adding oxygen to the source chamber of the mass spectrometer using a bleed valve ($P_{O_2} \sim 1 \times 10^{-7}$ mbar). Standards and samples are typically measured with a $^{182}WO_3^-$ beam intensity of ~1 V, for which stable W signal and low Re signal can be maintained over 8–12 h.

All measurements are performed using a two-line acquisition scheme. The Faraday cup assembly is centered at masses 231 and 233 amu, corresponding to $^{183}WO_3^-$ and $^{185}ReO_3^-$, respectively (Table A.1). This cup configuration allows simultaneous collection of all $W^{16}O_3^-$ species, as well as ReO_3^- species for monitoring Re interferences on masses 233 and 235. Interfering Ta and Os trioxides are also monitored on mass 229 and 236 during measurement, but never reach detectable level. For each measurement, 600–1200 ratios are collected with 8 s integration times in blocks of 20. For each block of data collection, the two peaks are centered, and the amplifiers are electronically rotated relative to the Faraday cup detectors. Also, 30 s of baseline measurement is made per block for each Faraday cup/amplifier pair by beam deflection. The ion beam is refocused every 3 blocks using the automated focus capability of the *Triton*. Prior to measurement, other masses (from 200 to 260) are scanned using the electron multiplier detector. Typically, there are no detectable interferences on W isotopes, except for Re.

3.2. Oxide interferences

The ionization of W as WO_3^- mainly results in the production of $W^{16}O_3^-$ but also, in smaller relative abundances, of other species, such as $W^{16}O_2{}^{17}O^-$, $W^{16}O^{17}O_2^-$, $W^{16}O^{18}O_2^-$, $W^{16}O^{17}O^{18}O^-$, $W^{17}O_3^-$ and $W^{17}O_2{}^{18}O^-$, that create isobaric interferences on the major isotopes measured. Other oxide species, such as $W^{17}O^{18}O_2^-$ and $W^{18}O_3^-$ are also formed, but they do not generate significant interferences because the atomic mass of W isotope range only over 4 amu (excluding ^{180}W which has low relative abundance). In addition, $^{185}Re^{16}O_2{}^{17}O^-$, derived from the ionization filament interferes with $^{186}W^{16}O_3^-$. The abundance of this Re oxide species is commonly insignificant (<10 ppm), relative to the abundance of the W oxide, as the $^{185}Re^{16}O_3^-$ signal can usually be maintained to levels one or two order of magnitude lower than the $^{186}W^{16}O_3^-$ signals. Measured intensity at mass x (^{x}I) derive from the combination of the signal due to $^{x-48}W^{16}O_3^-$ trioxide, and signals derived from other isobaric W and Re trioxides. The following oxide correction equations were developed earlier for Os and W isotope measurement by N-TIMS [25,32,33], interference corrected intensities at mass x, $^{x-48}W^{16}O_3$, are calculated as follows:

$$^{180}W^{16}O_3 = {}^{228}I$$

$$^{182}W^{16}O_3 = {}^{230}I - {}^{180}W^{16}O_3 \times 3\left[\left(\frac{^{17}O}{^{16}O}\right)^2 + \frac{^{18}O}{^{16}O}\right]$$

$$^{183}W^{16}O_3 = {}^{231}I - {}^{182}W^{16}O_3 \times 3\left(\frac{^{17}O}{^{16}O}\right) - {}^{180}W^{16}O_3 \times \left[6\left(\frac{^{17}O}{^{16}O}\right)\left(\frac{^{18}O}{^{16}O}\right) + \left(\frac{^{17}O}{^{16}O}\right)^3\right]$$

$$^{184}W^{16}O_3 = {}^{232}I - {}^{183}W^{16}O_3 \times 3\left(\frac{^{17}O}{^{16}O}\right) - {}^{182}W^{16}O_3 \times 3\left[\left(\frac{^{17}O}{^{16}O}\right)^2 + \frac{^{18}O}{^{16}O}\right] - {}^{180}W^{16}O_3 \times 3\left(\frac{^{18}O}{^{16}O}\right)\left[\left(\frac{^{17}O}{^{16}O}\right)^2 + \frac{^{18}O}{^{16}O}\right]$$

$$^{185}Re^{16}O_3 = {}^{233}I - {}^{184}W^{16}O_3 \times 3\left(\frac{^{17}O}{^{16}O}\right) - {}^{183}W^{16}O_3 \times 3\left[\left(\frac{^{17}O}{^{16}O}\right)^2 + \frac{^{18}O}{^{16}O}\right] - {}^{182}W^{16}O_3 \times \left[6\left(\frac{^{17}O}{^{16}O}\right)\left(\frac{^{18}O}{^{16}O}\right) + \left(\frac{^{17}O}{^{16}O}\right)^3\right]$$

$$^{186}W^{16}O_3 = {}^{234}I - {}^{185}Re^{16}O_3 \times 3\left(\frac{^{17}O}{^{16}O}\right) - {}^{184}W^{16}O_3 \times 3\left[\left(\frac{^{17}O}{^{16}O}\right)^2 + \frac{^{18}O}{^{16}O}\right] - {}^{183}W^{16}O_3 \times \left[6\left(\frac{^{17}O}{^{16}O}\right)\left(\frac{^{18}O}{^{16}O}\right) + \left(\frac{^{17}O}{^{16}O}\right)^3\right] - {}^{182}W^{16}O_3 \times 3\left(\frac{^{18}O}{^{16}O}\right)\left[\left(\frac{^{17}O}{^{16}O}\right)^2 + \frac{^{18}O}{^{16}O}\right]$$

Oxide interference corrections are initially estimated by assuming that W and Re are associated with O with an ambient isotopic composition ($^{17}O/^{16}O = 0.0003749$ and $^{18}O/^{16}O = 0.0020439$ [34]).

3.3. Mass fractionation correction

Instrumental fractionation is the major limiting factor precluding accurate determination of isotopic ratio by mass spectrometry. For thermal ionization sources, it is largely induced by preferential evaporation of light isotopes relative to heavier isotopes. As illustrated in Fig. A.1, this results in measured isotope ratios that display strongly correlated variations ($r^2 = 0.98$) when plotted on binary logarithmic diagrams. Within each run, fractionation increases with time, resulting in significant evolution of measured isotope ratios during the analysis. The effect of this mass-dependent fractionation can be corrected for a given isotope ratio (R^{xy}) by normalizing to a second ratio (R^{zw}) of two stable and non radiogenic isotopes (z and w) using the exponential law [35]:

$$R^{xy}_{zw} = R^{xy}_{m} \times \left(\frac{R^{zw}_{true}}{R^{zw}_{m}} \right)^{\ln(M_x/M_y)/\ln(M_z/M_w)}$$

where M corresponds to the atomic mass of the W trioxide species, R^{xy}_{zw} is the mass fractionation corrected ratio, obtained via normalization to R^{zw}, R^{xy}_{m}, and s is the measured ratio.

Tungsten consists of four stable, non-radiogenic isotopes, ^{180}W, ^{183}W, ^{184}W and ^{186}W, along with the radiogenic ^{182}W. The relative abundance of ^{180}W is too low to use to monitor fractionation. The other three isotopes provide two independent normalization options. Here, we used $^{186}W/^{184}W = 0.92767$ and $^{186}W/^{183}W = 1.9859$ as normalizing ratios [15]. After mass fractionation correction relative to $^{186}W/^{183}W$, correlations of isotope ratios and their variations with time disappear (Fig. A.2). Internal precisions of 3.6 and 2.6 ppm on corrected $^{182}W/^{184}W$ and $^{183}W/^{184}W$ ratios, respectively, are typically reached by the end of 1200 measurement cycles with a ~1 V ^{182}W beam, consistent with errors predicted by theoretical ion-counting statistics.

Small residual correlation ($r^2 = 0.49$) and temporal variations persist when the normalization relative to $^{186}W/^{184}W$ is applied. This likely reflects small variations in the isotopic composition of oxygen during the course of individual measurements. These changes have a larger effect on isotope ratios normalized to $^{186}W/^{184}W$ than on those normalized to $^{186}W/^{183}W$ (see Section 3.5, Fig. 1). Consequently, normalization to $^{186}W/^{183}W$ yields slightly lower internal precisions of 4.8 and 4.0 ppm on corrected $^{182}W/^{184}W$ and $^{183}W/^{184}W$ ratios, respectively.

3.4. Inter-collector biases

Inter-collector biases are an additional potential source of inaccuracy of isotope measurements that require corrections at the ±5 ppm precision level, as previously demonstrated for Nd and Sr isotopes [36–39]. These biases are related to efficiency variations between amplifiers and the deterioration of Faraday cups accompanying aging. The electronic amplifier rotation system of the *Triton* permits successive linkage of each cup to a different amplifier, and hence, cancels inter-amplifier biases. The effect of cup deterioration can be minimized by multi-dynamic isotope ratio collection, allowing mathematical elimination of relative variations of cup efficiencies. In multi-dynamic calculations [39], $^{182}W/^{184}W$ ratios measured on cups L1 and H1 (line 2) are corrected for mass fractionation using $^{186}W/^{184}W$ ratios measured on the same cups (line 1):

$$(R^{24}_{64})_{mdyn} = (R^{24}_{m})_{line2} \times \left(\frac{R^{64}_{true}}{(R^{64}_{m})_{line1}} \right)^{\ln(M_{182}/M_{184})/\ln(M_{186}/M_{184})}$$

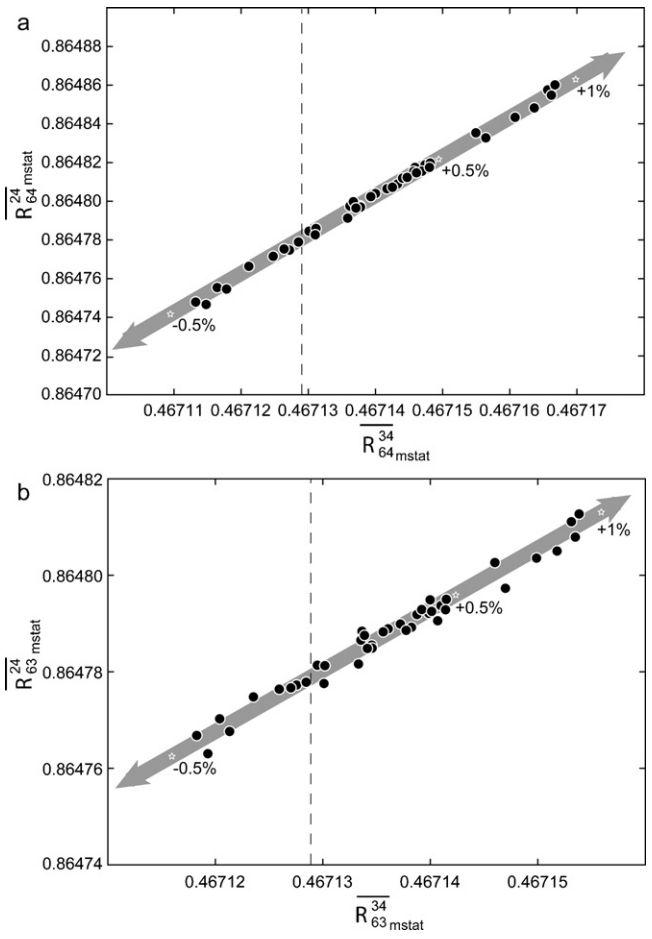

Fig. 1. Mass fractionation corrected $^{182}W/^{184}W$ dynamic average ratios ($\overline{R^{24}_{zw\,dyn}}$) versus corrected $^{183}W/^{184}W$ dynamic average ratios ($\overline{R^{34}_{zw\,dyn}}$) for 45 repeated analyses of 1.5 μg W *Alfa Aesar* standard solution. (a) Using normalization to $^{186}W/^{184}W$; (b) using normalization to $^{186}W/^{183}W$. Repeated measurements define linear trends that follow the theoretical effects of mass dependent oxygen fractionation (grey arrow), resulting in a change in the O isotope composition assumed for oxide interference corrections. Numeric labels correspond to relative variations of the $^{17}O/^{16}O$ ratio in percent. This second order instrumental fractionation is corrected by normalization to $^{183}W/^{184}W = 0.416729$, using a linear law.

An identical approach cannot be used to dynamically determine the $^{183}W/^{184}W$ ratio. Hence, multi-static W isotopes ratios, $(R^{24}_{zw})_{mstat}$ and $(R^{34}_{zw})_{mstat}$, are also calculated by averaging mass fractionation corrected isotope ratios obtained for both sequences of each measurement cycle. Although a multi-static calculation does not ensure complete elimination of Faraday cup biases, it can be applied to both $^{182}W/^{184}W$ and $^{183}W/^{184}W$ ratios, in contrast to multi-dynamic calculation, as follows:

$$(R^{xy}_{zw})_{mstat} = \frac{(R^{xy}_{zw})_{stat\,1} + (R^{xy}_{zw})_{stat\,2}}{2}$$

where the subscripts *mstat*, *stat 1* and *stat 2* refer to the multi-static ratio, static ratio measured on line 1, and static ratio measured on line 2.

Repeated measurements of the standard *Alfa Aesar* over a period of one year show significant correlated variations of $^{182}W/^{184}W$ and $^{183}W/^{184}W$ ratios (Fig. 1), resulting in external reproducibility that is much poorer than internal precision. Using normalization to $^{186}W/^{184}W$, static, multi-static, and multi-dynamic calculations yield a similar $^{182}W/^{184}W$ versus $^{183}W/^{184}W$ correlation with a slope of 2.07, and reduced external reproducibility on $^{182}W/^{184}W$ and $^{183}W/^{184}W$ ratios of ~60–70 ppm (Table A.2). In the same way, with normalization to $^{186}W/^{183}W$, all calculations yield a similar

correlation slope of 1.26 and reduced external reproducibility of ~30–40 ppm (Table A.3). Given that these variations are observed for static, multi-static, and multi-dynamic W isotope ratios, these variations cannot be well explained by relative variations of cup efficiencies.

3.5. Inaccurate fractionation correction?

Another possible cause of measurement imprecision is the method used for fractionation correction. At the ±5 ppm level of precision, the accuracy of the exponential fractionation law has been called into question [40–42]. Mixing of different filament domains exhibiting different degrees of isotopic depletion might result in non-exponential fractionation, which can eventually translate into linearly correlated variations of isotope ratios within an individual run, as suggested for Nd isotopes by these studies. However, this type of more complex fractionation would not necessarily translate into correlated variations for independently repeated measurements, as we observe for $^{182}W/^{184}W$ and $^{183}W/^{184}W$, unless isotopically depleted and enriched domains are generated with extreme reproducibility from one filament to another. In addition, in a plot of $^{182}W/^{184}W$ versus $^{183}W/^{184}W$, data normalized to $^{186}W/^{183}W$ and data normalized to $^{186}W/^{184}W$ plots along lines with different slopes (1.26 and 2.07, respectively). This observation cannot be explained by binary mixing, which would produce correlations with identical slopes for both normalizations. Hence, non-exponential fractionation of W isotope does not account for the correlated variations and reduced external reproducibility of $^{182}W/^{184}W$ and $^{183}W/^{184}W$ ratios observed for our repeated measurements.

3.6. Effects of changing oxygen isotope composition

In a plot of $^{182}W/^{184}W$ versus $^{183}W/^{184}W$ (Fig. 1), the standard measurements define a linear trend that mimics the theoretical effects of mass dependent change of O isotope composition used for calculating oxide interference corrections. As illustrated in Fig. 1, a minor variation of oxygen isotope composition of about 2% is sufficient to produce the residual observed variations in W isotope compositions. Effects of mass dependent oxygen fractionation on $^{182}W/^{184}W$ and $^{183}W/^{184}W$ ratios mainly depend on the isotope ratio used for mass fractionation correction. Isotope ratios normalized relative to $^{186}W/^{184}W$ indeed show larger variations than ratios normalized relative to $^{186}W/^{183}W$, consistent with a larger oxide isobaric interference correction on the signal measured at the $^{184}WO_3$ mass than at the $^{183}WO_3$ mass. Correlation between $^{182}W/^{184}W$ and $^{183}W/^{184}W$ ratios is not observed within each individual run for normalization to $^{186}W/^{183}W$, and only vaguely appears for normalization to $^{186}W/^{184}W$ (Fig. A.2). This suggests that the oxygen isotope composition of oxides ionized on the Re filament varies only marginally within each load through an analysis, but can significantly vary from one load to another. We suspect that the variations result from long term changes in the O isotopic compositions of loading materials, as well as changes in the proportions of the O supplied from the O bleed valve versus O contained within the loaded materials. This secondary instrumental fractionation can be eliminated by normalizing the $^{182}W/^{184}W$ ratio of each run to $^{183}W/^{184}W$ using a linear law, as follows:

$$\overline{R^{24}_{zw\,mtat}}^{true} = \overline{R^{24}_{zw\,mstat}} + m_{zw} \times (\overline{R^{34}}^{true} - \overline{R^{34}_{zw\,mstat}})$$

where $\overline{R^{24}_{zw\,mstat}}$ and $\overline{R^{34}_{zw\,mstat}}$ refer to the average, for each individual run, of mass fractionation corrected $^{182}W/^{184}W$ and $^{183}W/^{184}W$ multi-static ratios, respectively. The subscript *zw* indicates the normalizing ratio used for the mass fractionation correction ($^{186}W/^{184}W$ or $^{186}W/^{183}W$). $\overline{R^{24}_{zw\,mtat}}^{true}$ corresponds to the $^{182}W/^{184}W$ ratio of the individual run corrected for effect of oxygen isotope fractionation and $\overline{R^{34}}^{true}$ to the $^{183}W/^{184}W$ reference value. Here we choose $\overline{R^{34}}^{true} = 0.416729$, which yields consistent absolute values for $\overline{R^{24}_{64\,mtat}}^{true}$ and $\overline{R^{24}_{63\,mtat}}^{true}$. m_{zw} corresponds to the oxygen fractionation correction factor, and critically depends on the isotope ratio R^{zw} used for mass fractionation correction. This parameter can be evaluated by two different approaches. First, m_{zw} can be assumed to be identical from one measurement to another and, hence, to correspond to the slope of regressions obtained for repeated measurements of the *Alfa Aesar* standard in $^{182}W/^{184}W$ versus $^{183}W/^{184}W$ binary diagrams. This yields $m_{64} = 2.057539$ and $m_{63} = 1.232622$. m_{zw} also slightly varies depending on the magnitudes of the W and Re signals and, hence, from one run to another. Fortunately, m_{zw} can also be determined for each individual run by simulating the effect of mass dependent O fractionation on $\overline{R^{24}_{zw\,mstat}}$ and $\overline{R^{34}_{zw\,mstat}}$, and changing the O isotope composition assumed for oxide interference corrections (Tables 2 and 3). Overall, there is good agreement between m_{zw} values determined for individual runs (standards and samples), and the one derived from standard regression. The only exceptions are the few runs where the ^{185}Re signal did not drop below 100 mV. However, even in these cases, $\overline{R^{24}_{zw\,mstat}}^{true}$, calculated using m_{zw} derived from both approaches, are always consistent with each other within analytical uncertainties (Tables 2 and 3). Here we prefer to use the calculated individual m_{zw} for correcting the effects of O isotope composition variation, as it yields more reproducible $\overline{R^{24}_{zw\,mstat}}^{true}$ values. This is more important in the case of sample measurement, where Re signals are generally higher than for standard measurements (see Section 4.2).

The second-order correction for O isotope fractionation can also be applied to multi-dynamic $^{182}W/^{184}W$ ratios ($\overline{R^{24}_{64\,mdyn}}^{true}$). However, $^{183}W/^{184}W$ ratios cannot be dynamically determined using a similar approach, so that multi-dynamic $^{182}W/^{184}W$ ratios, $\overline{R^{24}_{64\,mdyn}}$, have to be normalized relative to multi-static $^{183}W/^{184}W$ ratios, $\overline{R^{34}_{64\,mstat}}$. Hence, second-order corrected multi-dynamic $^{182}W/^{184}W$ ratios yield an external reproducibility of ±10.5 ppm (Table A.4). It is better than non second-order corrected multi-dynamic data (±65.3 ppm) but not as good as second-order corrected multi-static data (±4.5 ppm). The reason for this remains unclear, as the multi-static approach does not allow elimination of Faraday cup biases in contrast multi-dynamic approach. Nevertheless, the results justify the use of multi-static calculation as our preferred approach. After second order correction, better external reproducibility of the multi-static data relative to multi-dynamic data could mostly reflect doubled integration time, consistent with an interpretation that cup deterioration on our instrument is currently a minor source of error. On the other hand, Faraday cup biases may also be partially cancelled when the second order correction is applied to multi-static data.

4. Results and discussion

4.1. Accuracy and reproducibility of W isotope measurements

After internal corrections for oxide interferences, for W isotope mass fractionation and for inter-collector biases, and finally external corrections for O isotope mass fractionation, our repeated measurements of the *Alfa Aesar* standard solution performed over a period of 9 months (Table 2 and Fig. 2) yields $^{182}W/^{184}W = 0.8647795 \pm 0.0000040$ (2σ SD, $n = 39$) for mass fractionation correction relative to $^{186}W/^{184}W$, and $^{182}W/^{184}W = 0.8647787 \pm 0.0000039$ (2σ SD, $n = 39$) for mass fractionation correction relative to $^{186}W/^{183}W$. This corresponds to a

Table 2
Results for the *Alfa Aesar* standard corrected using a double normalization procedure.

	Magazine	^{182}W(V)	^{185}Re(V)	m_{64}	m_{63}	$\overline{R^{24}_{64\,mstat}}^{true}$ [a]	±2σ	$\overline{R^{24}_{63\,mstat}}^{true}$ [a]	±2σ	$\overline{R^{24}_{64\,mstst}}^{true}$ [b]	±2σ	$\overline{R^{24}_{63\,mstat}}^{true}$ [b]	±2σ
S1	M0160	1.286	0.016	2.076812	1.252253	0.864782	0.000003	0.864781	0.000002	0.864782	0.000003	0.864781	0.000002
S2	M0160	1.202	0.013	2.084271	1.263526	0.864781	0.000003	0.864780	0.000002	0.864781	0.000003	0.864780	0.000002
S3	M0160	0.782	0.010	2.076669	1.252024	0.864782	0.000004	0.864782	0.000003	0.864782	0.000004	0.864782	0.000003
S4	M0160	1.112	0.018	2.076474	1.251754	0.864780	0.000003	0.864780	0.000002	0.864780	0.000003	0.864780	0.000002
S5	M0160	1.078	0.015	2.076774	1.252205	0.864782	0.000004	0.864781	0.000003	0.864782	0.000004	0.864781	0.000003
S6	M0164	1.078	0.015	2.076774	1.252205	0.864780	0.000004	0.864779	0.000003	0.864779	0.000004	0.864779	0.000003
S7	M0164	2.696	0.018	2.077363	1.253106	0.864781	0.000002	0.864780	0.000002	0.864780	0.000002	0.864780	0.000002
S8	M0164	4.840	0.027	2.076658	1.253531	0.864782	0.000002	0.864781	0.000002	0.864782	0.000002	0.864781	0.000002
S9	M0169	2.164	0.016	2.078756	1.255355	0.864778	0.000003	0.864779	0.000002	0.864778	0.000003	0.864779	0.000002
S10	M0169	2.801	0.022	2.084901	1.265422	0.864778	0.000004	0.864776	0.000003	0.864778	0.000004	0.864776	0.000003
S11	M0171	3.615	0.031	2.077541	1.253377	0.864779	0.000002	0.864778	0.000001	0.864779	0.000002	0.864778	0.000001
S12	M0171	3.078	0.024	2.084213	1.264045	0.864778	0.000002	0.864778	0.000001	0.864778	0.000002	0.864778	0.000001
S13	M0172	1.922	0.015	2.084759	1.264214	0.864782	0.000003	0.864781	0.000002	0.864782	0.000003	0.864781	0.000002
S14	M0172	3.081	0.019	2.084931	1.264566	0.864781	0.000002	0.864781	0.000002	0.864781	0.000002	0.864781	0.000002
S15	M0172	0.864	0.017	2.083159	1.261885	0.864780	0.000007	0.864779	0.000005	0.864780	0.000007	0.864779	0.000005
S16	M0173	1.506	0.014	2.076987	1.252550	0.864775	0.000006	0.864775	0.000005	0.864776	0.000006	0.864775	0.000005
S18	M0173	3.397	0.020	2.085838	1.265163	0.864780	0.000002	0.864780	0.000002	0.864780	0.000002	0.864780	0.000002
S19	M0173	2.274	0.019	2.085051	1.264028	0.864777	0.000002	0.864777	0.000002	0.864777	0.000002	0.864777	0.000002
S19	M0174	2.047	0.028	2.084488	1.263883	0.864779	0.000003	0.864778	0.000002	0.864779	0.000003	0.864778	0.000002
S20	M0174	2.209	0.030	2.084439	1.263777	0.864783	0.000003	0.864781	0.000002	0.864783	0.000003	0.864781	0.000002
S21	M0174	3.203	0.038	2.085627	1.264262	0.864781	0.000002	0.864780	0.000001	0.864780	0.000002	0.864780	0.000001
S22	M0174	2.563	0.032	2.084963	1.263532	0.864779	0.000002	0.864778	0.000002	0.864779	0.000002	0.864778	0.000002
S23	M0174	1.208	0.016	2.084469	1.263807	0.864778	0.000003	0.864776	0.000002	0.864778	0.000003	0.864776	0.000002
S24	M0175	2.294	0.023	2.084687	1.266504	0.864781	0.000004	0.864781	0.000003	0.864781	0.000004	0.864781	0.000003
S25	M0176	1.505	0.019	2.084968	1.264503	0.864780	0.000004	0.864778	0.000003	0.864780	0.000004	0.864778	0.000003
S26	M0176	1.780	0.023	2.085114	1.264006	0.864781	0.000003	0.864781	0.000002	0.864780	0.000003	0.864780	0.000002
S27	M0176	1.161	0.019	2.085006	1.263686	0.864777	0.000003	0.864778	0.000002	0.864776	0.000003	0.864777	0.000002
S28	M0176	2.048	0.028	2.085440	1.263809	0.864778	0.000003	0.864778	0.000002	0.864777	0.000003	0.864777	0.000002
S29	M0177	3.146	0.026	2.084270	1.264213	0.864779	0.000002	0.864778	0.000001	0.864778	0.000002	0.864777	0.000001
S30	M0177	2.740	0.022	2.084629	1.264056	0.864780	0.000002	0.864780	0.000002	0.864779	0.000002	0.864779	0.000002
S31	M0177	2.296	0.017	2.084595	1.263088	0.864780	0.000002	0.864780	0.000002	0.864780	0.000002	0.864779	0.000002
S32	M0177	1.489	0.013	2.084427	1.263771	0.864779	0.000003	0.864778	0.000002	0.864778	0.000003	0.864777	0.000002
S33	M0177	1.090	0.017	2.083718	1.261979	0.864779	0.000003	0.864780	0.000003	0.864779	0.000003	0.864780	0.000003
S34	M0177	1.581	0.009	2.084704	1.264206	0.864777	0.000003	0.864776	0.000002	0.864776	0.000003	0.864776	0.000002
S35	M0178	3.500	0.026	2.084525	1.264314	0.864779	0.000002	0.864779	0.000001	0.864778	0.000002	0.864778	0.000001
S36	M0178	1.059	0.014	2.084204	1.262665	0.864782	0.000004	0.864782	0.000003	0.864781	0.000004	0.864781	0.000003
S37	M0178	3.524	0.028	2.084945	1.264535	0.864776	0.000004	0.864775	0.000002	0.864775	0.000004	0.864774	0.000002
S38	M0178	1.190	0.012	2.085361	1.264445	0.864776	0.000004	0.864777	0.000003	0.864775	0.000004	0.864776	0.000003
S39	M0179	1.474	0.017	2.084158	1.263355	0.864778	0.000003	0.864777	0.000002	0.864777	0.000003	0.864777	0.000002
Mean						0.864779	0.000004	0.864779	0.000004	0.864779	0.000004	0.864779	0.000004
2σ SD (ppm) $n = 39$						4.5		4.5		4.6		4.6	

[a] Calculated using the second order normalization parameters, $m_{64} = 2.057539$ and $m_{63} = 1.232622$, estimated from regression of *Alfa Aesar* standard measurements.

[b] Calculated using m_{64} and m_{63} values shown here, and determined for each individual by changing the O isotope composition assumed for oxide interference corrections according to terrestrial mass fractionation.

Table 3
Results for the standard-spike mixture (S–S mix) and basalt LP15 corrected using double normalization procedure.

	Magazine	^{182}W(V)	^{185}Re(V)	m_{64}	m_{63}	μ^{24}_{64} [a]	±2σ	μ^{24}_{63} [a]	±2σ	μ^{24}_{64} [b]	±2σ	μ^{24}_{63} [b]	±2σ
S–S mix 1	M0169	1.709	0.015	2.084726	1.265198	12.5	4.9	13.6	3.2	12.7	4.9	13.7	3.2
S–S mix 2	M0169	3.633	0.017	2.085225	1.264916	11.1	4.1	9.4	2.8	10.6	4.1	9.0	2.8
S–S mix 3	M0174	1.130	0.023	2.083659	1.262572	13.1	7.0	14.8	5.8	12.5	7.0	14.2	5.8
S–S mix 4	M0177	1.502	0.009	2.078470	1.254687	14.2	6.9	14.1	4.6	13.9	6.9	13.9	4.6
S–S mix 5	M0177	1.177	0.010	2.085541	1.265431	10.6	8.0	10.2	5.5	10.5	8.0	10.0	5.5
S–S mix 6	M0179	0.491	0.008	2.085541	1.265431	9.2	7.5	12.6	5.5	9.2	7.5	12.6	5.5
S–S mix 7	M0179	2.365	0.013	2.085541	1.265431	10.3	3.3	10.2	2.3	9.9	3.3	9.9	2.3
Mean – 2σ SD n = 7						11.5	3.5	12.1	4.3	11.3	3.4	11.9	4.4
LP15 (1)	M0171	0.817	0.325	2.035062	1.189816	−3.7	6.3	−0.6	4.7	−3.4	6.3	−0.4	4.7
LP15 (2)	M0171	0.954	0.375	2.030279	1.185503	2.6	4.8	1.3	3.7	3.4	4.8	2.0	3.7
LP15 (3)	M0171	1.162	0.243	2.057055	1.212928	1.2	7.2	−1.2	5.4	1.6	7.2	−0.6	5.4
Mean – 2σ SD n = 3						0.0	6.6	−0.2	2.6	0.5	7.0	0.4	2.9
Processed standard	M0159	1.128	0.095	2.068961	1.240507	1.0	4.1	−0.2	3.1	1.1	4.1	−0.1	3.1

[a] Calculated using second order normalization parameters, m_{64} = 2.057539 and m_{63} = 1.232622, estimated from regression of *Alfa Aesar* standard measurements.
[b] Calculated using m_{64} and m_{63} values shown here, and determined for each individual by changing the O isotope composition assumed for oxide interference corrections according to terrestrial mass fractionation.

long-term external reproducibly of ±4.5 ppm (2σ SD, n = 39) for both normalizations. Here, we use the μ^{182}W notation, which corresponds to the deviation of ^{182}W/^{184}W ratio of a sample, $(\overline{R^{24}_{zw\,mstat}}^{true})_{sample}$, relative to average isotope ratio calculated for the 39 repeated *Alfa Aesar* standard measurements, $(\overline{R^{24}_{zw\,mstat}}^{true})_{standard}$, in part per million.

$$\mu^{182}W^{sample}_{zw} = \left[\frac{(\overline{R^{24}_{zw\,mstat}}^{true})_{sample}}{(\overline{R^{24}_{zw\,mstat}}^{true})_{standard}} - 1\right] \times 10^6$$

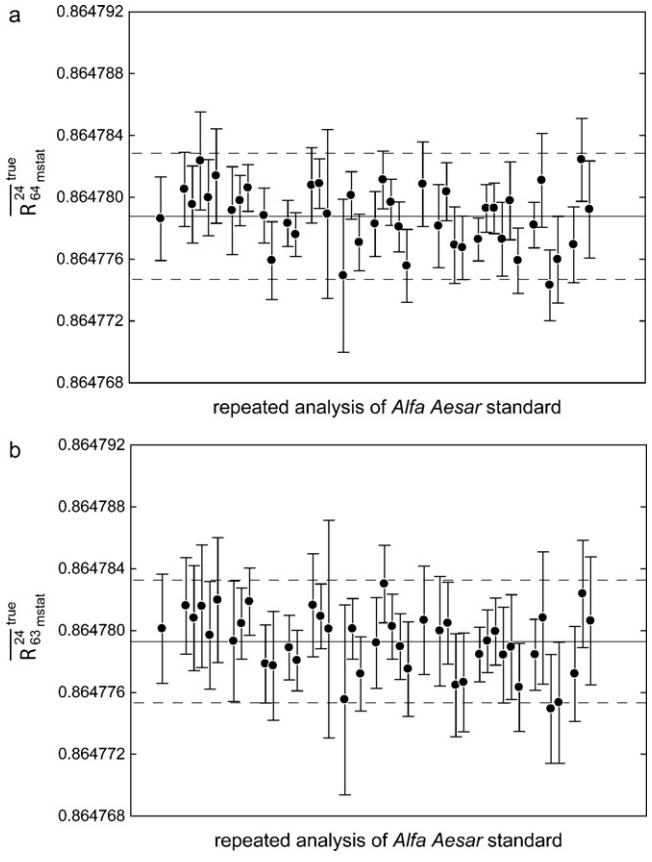

Fig. 2. Long-term external reproducibility of ^{182}W/^{184}W dynamic ratios for 45 repeated analyses of 1.5 μg W *Alfa Aesar* standard solution after correction for second order instrumental fractionation. (a) Using first order normalization to ^{186}W/^{184}W ($\overline{R^{24}_{64\,true}}$). (b) Using first order normalization to ^{186}W/^{183}W ($\overline{R^{24}_{63\,true}}$). With both double normalization procedures, an external reproducibility of ^{182}W/^{184}W ratio better 5 ppm is achieved.

The accuracy of our ^{182}W/^{184}W analysis is monitored by measuring a gravimetrically prepared mixture of W standard and ^{182}W-enriched spike (Table 3 and Fig. 3). The standard-spike mixture was prepared in order to generate a +10.3 ppm ^{182}W positive anomaly. Repeated measurements of the mixture yielded $\mu^{182}W_{64}$ = +11.3 ± 3.4 ppm and $\mu^{182}W_{63}$ = +11.9 ± 4.4 ppm (2σ SD, n = 7), which is in good agreement with the gravimetric calculation. The standard, processed through our four-step ion chromatography protocol (Table 1), shows an identical W isotope composition ($\mu^{182}W_{64}$ = 1.1 ± 4.1 ppm and $\mu^{182}W_{63}$ = −0.1 ± 3.1 ppm) compared to the unprocessed standard, indicating that no W isotope fractionation was introduced by the chemical procedure at the ±4.5 ppm precision level.

4.2. Tungsten isotope measurements of natural samples

Replicated analysis of the modern terrestrial basalt La Palma 15 [30] for distinct dissolutions permits assessment of accuracy and external reproducibility of our method for typical geological samples. Results are presented in Supplemental Tables A.5 and A.6, Table 3 and Fig. 3. Due to somewhat higher Re residual signals present though sample measurements, the effects of O isotope fractionation on W isotope ratios changed slightly compared to the effects for standard measurements. This translates into small differences between the O fractionation correction factors, m_{zw}, determined from individual measurements (Table 3) and those derived from standard regression (m_{64} = 2.057539 and m_{63} = 1.232622). Both approaches for correcting for secondary instrumental fractionation yield consistent estimates of W isotope composition for La Palma 15 that are both identical to the isotope composition of the *Alfa Aesar* standard within ±4.5 ppm. Better external reproducibility is observed when m_{zw} values, derived from each individual run, are used for normalization to ^{183}W/^{184}W (Table 3). This approach constitutes a better record of secondary instrumental fractionation correction, which varies as a function of the relative magnitude of W and Re oxide signals. It gives $\mu^{182}W_{64}$ = 0.5 ± 7.0 ppm and $\mu^{182}W_{63}$ = 0.4 ± 2.9 ppm (2σ SD, n = 3), which, therefore, is our best estimate for repeated analysis of

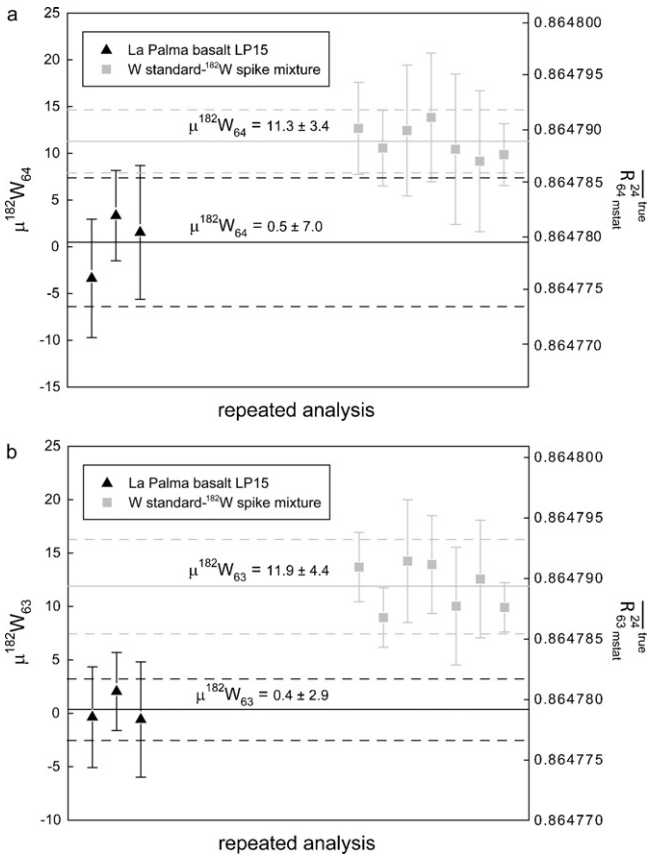

Fig. 3. $^{182}W/^{184}W$ ratios for repeated analyses of our in-house standard-spike mixture and of the basalt La Palma 15. (a) Using a first order normalization to $^{186}W/^{184}W$ ($\mu^{182}W_{64}$). (b) Using a first order normalization to $^{186}W/^{183}W$ ($\mu^{182}W_{63}$). The standard-spike mixture shows an ~11 ppm ^{182}W positive anomaly, identical within uncertainties to the gravimetric prediction (+10.3 ppm). The basalt has an identical composition to the *Alfa Aesar* standard.

the La Palma basalt. This result highlights the accuracy and reproducibility of the new W isotope measurement method by N-TIMS at the 4.5 ppm level for natural samples, which is comparable to what is observed for the W standard solution.

5. Conclusions

We have developed a new technique for the measurement of W as WO_3^- by N-TIMS using a *Thermo-Fisher Triton* mass spectrometer. The technique achieves a long-term external reproducibility of the $^{182}W/^{184}W$ ratio of ±4.5 ppm for about 1.5 μg of W purified from geological samples. The mass spectrometry protocol involves a two-line dynamic acquisition scheme and amplifier rotation for eliminating amplifier biases, and a double normalization procedure to account for instrumental fractionation on isotopes of both W and oxygen. This method represents a precision improvement by a factor ~5 compared to conventional W isotope measurement method by MC-ICPMS.

Acknowledgments

This work has been supported by NSF CSEDI grant 0757808 and NASA grant NNX10AG94G. We would like to thank James D. Day for providing the La Palma basalt, Richard Ash for assistance with ICPMS instruments, and Igor S. Puchtel for helpful discussion and assistance in the chemistry labs. We thank Richard Carlson, Klaus Metzger and one anonymous reviewer for their thorough and constructive reviews, which helped to improve the quality of the manuscript.

Appendix A. Supplementary data

Supplementary data associated with this article can be found, in the online version, at doi:10.1016/j.ijms.2011.08.033.

References

[1] C. Vockenhuber, F. Oberli, M. Bichler, I. Ahmad, G. Quitté, M. Meier, A.N. Halliday, D.C. Lee, W. Kutschera, P. Steier, R.J. Gehrke, R.G. Helmer, New half-life measurement of ^{182}Hf: improved chronometer for the early solar system, Phys. Rev. Lett. 93 (2004) 172501.
[2] H. Palme, W. Rammensee, The significance of W in planetary differentiation processes: evidence from new data on eucrites, Proc. Lunar Planet. Sci. 12B (1981) 949–964.
[3] H.E. Newsom, H. Palme, The depletion of siderophile elements in the Earth's mantle: new evidence from molybdenum and tungsten, Earth Planet. Sci. Lett. 69 (1984) 354–364.
[4] H.E. Newsom, Accretion and core formation in the Earth: evidence from siderophile elements, in: H.E. Newsom, J.H. Jones (Eds.), Origin of the Earth, Oxford University Press, 1990, pp. 273–288.
[5] K.W.W. Sims, H.E. Newsom, E. Gladney, Chemical fractionation during formation of the Earth's core and continental crust: clues from As, Sb W and Mo, in: H.E. Newsom, J.H. Jones (Eds.), Origin of the Earth, Oxford University Press, 1990, pp. 291–317.
[6] M.J. Walter, Y. Thibault, Partitioning of tungsten and molybdenum between metallic liquid and silicate melt, Science 270 (1995) 1186–1189.
[7] H.E. Newsom, K.W.W. Sims, P. Noll, W. Jaeger, S. Maehr, T. Beserra, The depletion of W in the bulk silicate Earth: constraints on core formation, Geochim. Cosmochim. Acta 60 (1996) 1155–1169.
[8] M.J. Walter, H.E. Newsom, W. Ertel, A. Holzheid, Siderophile elements in the Earth and Moon: metal/silicate partitioning and implications for core formation, in: R.M. Canup, K. Righter (Eds.), Origin of the Earth and Moon, Lunar and Planetary Institute, Houston, 2000.
[9] R. Schoenberg, B.S. Kamber, K.D. Collerson, S. Moorbath, Tungsten isotope evidence from ~3.8 Gyr metamorphosed sediments for early bombardment of the Earth, Nature 418 (2002) 403–405.
[10] A. Shérsten, T. Eliott, C. Hawkesworth, M. Norman, Tungsten isotope evidence that mantle plumes contain no contribution from the Earth's core, Nature 427 (2004) 234–237.
[11] Y.V. Sahoo, S. Nakai, A. Ali, Modified ion exchange separation for tungsten isotopic measurements from kimberlite samples using multi-collector inductively coupled plasma spectrometry, Analyst 131 (2006) 434–439.
[12] T. Iizuka, S. Nakai, Y.V. Sahoo, A. Takamasa, T. Hirata, S. Maruyama, The tungsten isotopic composition of eoarchean rocks: implications for early silicate differentiation and core–mantle interaction, Earth Planet. Sci. Lett. 291 (2010) 189–200.
[13] F. Moynier, Q.-Z. Yin, K. Irisawa, M. Boyet, B. Jacobsen, M.T. Rosing, Coupled ^{182}W–^{142}Nd constraint for early Earth differentiation, Proc. Natl. Acad. Sci. U. S. A. 107 (2010) 10810–10814.
[14] T. Kleine, C. Münker, K. Mezger, H. Palme, Rapid accretion and early core formation on asteroids and the terrestrial planets from Hf–W chronometry, Nature 418 (2002) 952–955.
[15] T. Kleine, K. Mezger, C. Münker, H. Palme, A. Bischoff, ^{182}Hf–^{182}W isotope systematics of chondrites, eucrites, and Martian meteorites: Chronology of core formation and mantle differentiation in Vesta and Mars, Geochim. Cosmochim. Acta 68 (2004) 2935–2946.
[16] Q.-Z. Yin, S.B. Jacobsen, K. Yamashita, J. Blichert-Toft, P. Telouk, F. Albarede, A short timescale for terrestrial planet formation from Hf–W chronometry of meteorites, Nature 418 (2002) 949–952.
[17] C. Burkhardt, T. Kleine, H. Palme, B. Bourdon, J. Zipfel, J. Friedrich, D. Ebel, Hf–W mineral isochron for Ca,Al-rich inclusions: age of the solar system and the timing of core formation in planetesimals, Geochim. Cosmochim. Acta 72 (2008) 6177–6197.
[18] A.N. Halliday, Mixing, volatile loss and compositional change during impact-driven accretion of the Earth, Nature 427 (2004) 505–509.
[19] S.B Jacobsen, The Hf–W isotopic system and the origin of the Earth and Moon, Ann. Rev. Earth Planet. Sci. 33 (2005) 531–570.
[20] K. Righter, C.K. Shearer, Magmatic fractionation of Hf and W: constraints on the timing of core formation and differentiation in the Moon and Mars, Geochim. Cosmochim. Acta 67 (2003) 2497–2507.
[21] M. Touboul, T. Kleine, B. Bourdon, H. Palme, R. Wieler, Late formation and prolonged differentiation of the Moon inferred from W isotopes in lunar metals, Nature 450 (2007) 1206–1209.
[22] B. Bourdon, M. Touboul, G. Caro, T. Kleine, Early stages of Earth and Moon evolution, Philos. Trans. R. Soc. A 366 (2008) 4105–4128.
[23] M. Touboul, T. Kleine, B. Bourdon, H. Palme, R. Wieler, Tungsten isotopes in ferroan anorthosites: implications for the age of the Moon and the lifetime of its magma ocean, Icarus 199 (2009) 245–249.

[24] R.J. Walker, Highly siderophile elements in the Earth, Moon and Mars: update and implications for planetary accretion and differentiation, Chem. Erde 69 (2009) 101–125.
[25] C.L. Harper, S.B. Jacobsen, Evidence for ^{182}Hf in the early Solar System and constraints on the timescale of terrestrial accretion and core formation, Geochim. Cosmochim. Acta 60 (1996) 1131–1153.
[26] M.F. Horan, M.I. Smoliar, R.J. Walker, ^{182}W and ^{187}Re–^{187}Os systematics of iron meteorites: chronology for melting, differentiation, and crystallization in asteroids, Geochim. Cosmochim. Acta 62 (1998) 545–554.
[27] K.G. Heumann, M. Köppe, M. Wachsmann, New developments in negative thermal ionization mass spectrometry and its applications, in: Proc. 37th ASMS Conf. Mass Spectrometry and Allied Topics, 1989, pp. 414–416.
[28] J. Völkening, M. Köppe, K.G. Heumann, Tungsten isotope ratio determinations by negative thermal ionization mass spectrometry, Int. J. Mass Spectrom. Ion Processes 107 (1991) 361–368.
[29] D.C. Lee, A.N. Halliday, Hf–W isotopic evidence for rapid accretion and differentiation in the early solar system, Science 274 (1996) 1876–1879.
[30] J.M.D. Day, D.G. Pearson, C.G. Macpherson, D.J.-C. Lowry, Carracedo pyroxenite-rich mantle formed by recycled oceanic lithosphere: oxygen-osmium isotope evidence from Canary Island lavas, Geology 37 (2009) 555–558.
[31] C. Münker, S. Weyer, E. Scherer, K. Mezger, Separation of high field strength elements (Nb, Ta, Zr, Hf) and Lu from rock samples for MC-ICPMS measurements, Geochem. Geophys. Geosyst. 2 (2001) 1064.
[32] R.A. Creaser, D.A. Papanastassiou, G.J. Wasserburg, Negative thermal ion mass spectrometry of osmium, rhenium and iridium, Geochim. Cosmochim. Acta 55 (1991) 397–401.
[33] A. Luguet, G.M. Nowell, D.G. Pearson, ^{184}Os/^{188}Os and ^{186}Os/^{188}Os measurements by Negative Thermal Ionisation Mass Spectrometry (N-TIMS): effects of interfering element and mass fractionation corrections on data accuracy and precision, Chem. Geol. 248 (2008) 342–362.
[34] A.O. Nier, A redetermination of the relative abundances of the isotopes of carbon, nitrogen, oxygen, argon, and potassium, Phys. Rev. 77 (1950) 789–793.
[35] W.A. Russell, D.A. Papanastassiou, T.A. Tombrello, Ca isotope fractionation in the Earth and other solar system materials, Geochim. Cosmochim. Acta 42 (1978) 1075–1090.
[36] M. Boyet, J. Blichert-Toft, M. Rosing, M. Storey, P. Télouk, F. Albarède, ^{142}Nd evidence for early Earth differentiation, Earth Planet. Sci. Lett. 214 (2003) 427–442.
[37] G. Caro, B. Bourdon, J.-L. Birck, S. Moorbath, High-precision ^{142}Nd/^{144}Nd measurements in terrestrial rocks: constraints on the early differentiation of the Earth's mantle, Geochim. Cosmochim. Acta 70 (2006) 164–191.
[38] U. Hans, T. Kleine, B. Bourdon, Rb–Sr chronology of volatile depletion of the angrite and eucrite parent bodies, 41st Lunar Planet, Sci. Conf. (2010) A1533.
[39] M.F. Thirlwall, Long-term reproducibility of multicollector Sr and Nd isotope ratio analysis, Chem. Geol. 94 (1991) 85–104.
[40] S.R. Hart, A. Zindler, Isotope fractionation laws: a test using calcium, Int. J. Mass Spectrom. Ion Processes 89 (1989) 287–301.
[41] D. Upadhyay, E.E. Scherer, K. Mezger, Fractionation and mixing of Nd isotopes during thermal ionization mass spectrometry: implications for high precision ^{142}Nd/^{144}Nd analyses, J. Anal. At. Spectrom. 23 (2008) 561–568.
[42] R. Andreasen, M. Sharma, Fractionation and mixing in a thermal ionization mass spectrometer source: implications and limitations for high-precision Nd isotope analyses, Int. J. Mass Spectrom. 285 (2009) 49–57.